1   Reduction in Earth Reflected Radiance during the Eclipse of 21 August 2017

2   Jay Herman[1], Guoyong Wen[2], Alexander Marshak[3], Karin Blank[3], Liang Huang[4], Alexander Cede[5], Nader
3   Abuhassan[1], Matthew Kowalewski[6]

4   Abstract

5   Ten wavelength channels of calibrated radiance image data from the Sunlit Earth are obtained
6   every 65 minutes during Northern Hemisphere summer from the DSCOVR/EPIC instrument located near
7   the Earth-Sun Lagrange-1 point (L_1), 1.5 million km from the Earth. The L_1 location permitted seven
8   observations of the Moon's shadow on the Earth for about 3 hours during the 21 August 2017 eclipse.
9   Two of the observations were timed to be over Casper, Wyoming and Columbia, Missouri. Since, the
10   solar irradiances within 5 channels (λ_i = 388, 443, 551, 680, and 780 nm) are not strongly absorbed in
11   the atmosphere, they can be used for characterizing eclipse reduction in reflected radiances for the
12   sunlit face of the Earth containing the eclipse shadow. Five channels (λ_i = 317.5, 325, 340, 688, and 764
13   nm) that are partially absorbed in the atmosphere give consistent reductions compared to the non-
14   absorbed channels. This indicates that cloud reflectivities dominate the 317.5 to 780 nm radiances
15   reflected back to space from the sunlit Earth's disk with a strong contribution from Rayleigh scattering
16   for the shorter wavelengths. A reduction of 9.7±1.7 % in the radiance (387 to 781 nm) reflected from the
17   Earth towards L_1 was obtained for the set of observations on 21 August 2017, while the shadow was in
18   the vicinity of Casper, Wyoming (42.8666° N, 106.3131° W, centered on 17:44:50 UTC). In contrast,
19   when successive non-eclipse days are compared for each wavelength channel, the change in reflected
20   light is much smaller (less than 1 % for 443 nm compared to 9 % during the eclipse). Also measured was
21   the spatially averaged ratio $<R_{EN}(\lambda_i)>$ of reflected radiance within the eclipse totality region to radiances
22   for the same geometry on adjacent non-eclipse days for all 10 wavelength channels. The measured
23   $<R_{EN}(443\ nm)>$ was smaller for Columbia (35) than for Casper (122), because Columbia had more cloud
24   cover than Casper. $R_{EN}(\lambda_i)$ forms a useful test of 3-D radiative transfer models for an eclipse in the
25   presence of optically thin clouds. A previously published clear-sky model (Emde and Mayer, 2007) shows
26   results for a nearly overhead eclipse had $R_{EN}(340nm)=1.7\times10^4$ compared to the maximum measured
27   non-averaged $R_{EN}(340)$ at Casper of 515±27 with optically thin clouds under similar geometrical
28   conditions.

29   Keywords: Atmospheric Processes, Eclipse, DSCOVR/EPIC, Reflected Energy

30   **Correspondence email: jay.r.herman@nasa.gov**

31

32   **[1]University of Maryland Baltimore County JCET**
33   **[2]Morgan State University, Baltimore Maryland**
34   **[3]NASA Goddard Space Flight Center, Greenbelt, Maryland**
35   **[4]Science Systems and Applications, Lanham, Maryland**
36   **[5]Goddard Earth Sciences Technology & Research (GESTAR) Columbia, Columbia, MD 21046, USA**
37   **[6]SciGlob Instruments and Services, Elkridge, Maryland USA**

38
39
40 **1.0 Introduction**

41   Measured radiances are presented during the 21 August 2017 eclipse from the DSCOVR (Deep Space
42 Climate Observatory) satellite synoptic observations of the entire sunlit Earth. DSCOVR observes the
43 earth from an orbit around the L_1 point (Lagrange 1) 1.5 million km from Earth (Herman et al., 2017).
44 This study focuses on data from two selected locations during the 21 August 2017 eclipse that crossed
45 the United States from west to east. The locations selected were Casper, Wyoming and Columbia,
46 Missouri, both near the center of the path of totality and both with a nearly overhead total solar eclipse
47 (local time 11:45 in Casper, Wyoming and 13:12 in Columbia, Missouri). The sites were selected in
48 advance to have a high probability of almost cloud-free skies, and so that totality would occur about 30
49 minutes apart (UTC, Coordinated Universal Time) to accommodate the satellite's ability to acquire data.
50 On the day of the eclipse, Casper, Wyoming had almost clear skies (Fig. 1), with some high thin clouds
51 visible, while Columbia, Missouri had thin low altitude cloud cover (Fig. 2).

52   Observations of total solar eclipses have been made with varying degrees of sophistication for
53 thousands of years as reviewed by Littman et al. (2008). At a given location, observations of reduced
54 irradiance reaching the Earth's surface are limited to just a few minutes of totality and about two hours
55 of partial obscuration (Meeus, 2003). The totality region (umbra) is about 250 to 267 km in diameter, if
56 it was near the center of the Earth's disk, but will change size and shape as a function of solar zenith
57 angle. Some of the complicating factors concerning quantitative eclipse observations include the effects
58 of the solar corona and light scattered in the atmosphere (Liendo, and Chacin, 2004; Emde and Mayer,
59 2007).

60   A detailed analysis of an eclipse that occurred in 2006 over southern Europe includes both ground-
61 based and space-based polar orbiting MODIS (Moderate Resolution Imaging Spectroradiometer)
62 observations (Gerasopoulos et al., 2008) as well as theoretical modelling of the eclipse, but unlike the
63 present study, it was largely limited to local effects near the region of totality. A comparison from a
64 meteorological radiation model and measurements of total solar irradiance were made near Athens
65 Greece (84 % of total eclipse) that showed good agreement in the presence of light clouds (Psiloglou and
66 Kambezidis, 2007). A 3D Monte Carlo radiative transfer study (Emde and Mayer, 2007) was applied to
67 the geometry for the nearly overhead total eclipse of 29 March 2006 (13:20 local time in Turkey), but
68 without the effect of clouds included in the calculation. Successful modelling of an eclipse under realistic
69 conditions is the first step to improved modelling of high cloud reflection and shadowing of solar
70 radiation on the Earth's energy balance.

71   The observations from the DSCOVR satellite are part of a larger project that combines
72 simultaneously obtained satellite and ground-based measurements using a pyranometer (Ji and Tsay,
73 2000) and the Pandora Spectrometer Instrument (Herman et al., 2009) at both sites. The combination
74 will be use to help validate three dimensional (3D) radiative transfer models applicable to analysis of
75 eclipse effects on radiances reflected back to space and reaching the Earth's surface. This study presents
76 the only synoptic satellite data of the sunlit Earth ever obtained during an eclipse, which should place

77 tighter limits on validating radiative transfer studies under realistic conditions that includes clouds,
78 aerosols, and surface reflectivity.

79

80   DSCOVR observations of the entire sunlit Earth from the eclipse day, 21 August 2017, are compared
81 to those from non-eclipse days to quantify the change of global averaged reflected solar radiation
82 caused by the eclipse. We present a potential validation test data set for the 21 August 2017 eclipse for
83 3D radiative transfer models, the ratio of radiances in the region of totality to radiances for the same
84 region without the eclipse on previous and following days, based on a suggestion in the paper by Emde
85 and Mayer (2007).
86
87   Section 2 describes the DSCOVR/EPIC instrument, available data, and monochromatic images based
88 on measured counts per second, C/s. Section 3.1 presents a comparison between eclipse and non-
89 eclipse days. Section 3.2 gives an estimate of the global reduction of reflected sunlight during the eclipse
90 over Casper, WY.
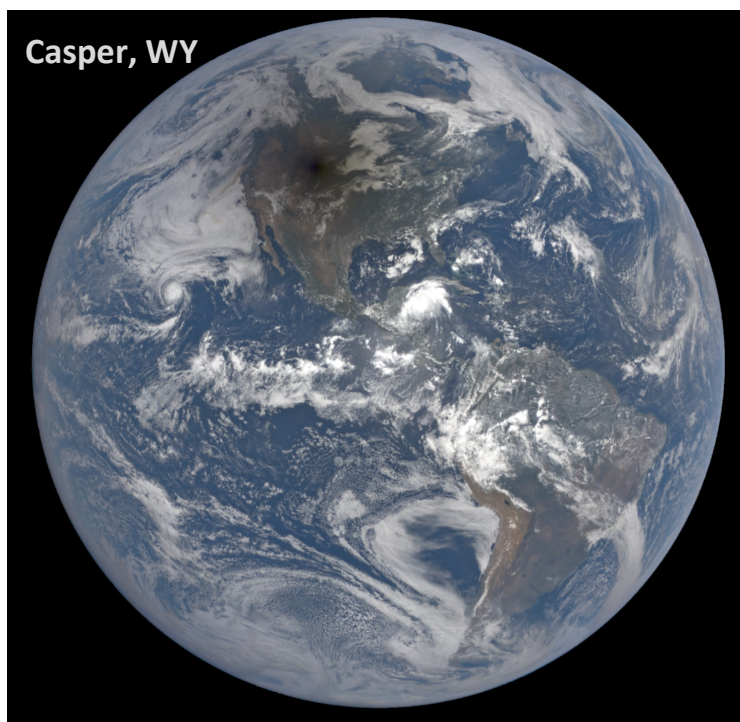
Fig. 01 Synoptic view of the sunlit Earth perturbed by the 21 August 2017 total eclipse centered over Casper, Wyoming at 17:44:50 UTC. The black region is the eclipse umbra centered over Casper, WY. The color image has been adjusted from the images on https://epic.gsfc.nasa.gov/ by increasing the gamma correction to bring out the region of totality and surrounding clouds.

91

Fig. 02 Synoptic view of the total eclipse centered over Columbia, Missouri at 18:14:50 UTC. The black region is the eclipse umbra centered over Casper, WY. The color image has been adjusted from the images on https://epic.gsfc.nasa.gov/ by increasing the gamma correction to bring out the region of totality and surrounding clouds.

92

93 **2.0 EPIC Instrument and Data Description**

94   The EPIC (Earth Polychromatic Imaging Camera) onboard the DSCOVR (Deep Space Climate
95 Observatory) spacecraft orbiting since June 2015 near the Lagrange-1 point (L_1 point 1.5 million km from
96 the Earth) observed the Moon's shadow for about 3 hours. The data comprises a set of seven
97 observations (16:44 to 19:44 UTC) starting in the Pacific Ocean and ending in the Atlantic Ocean, while
98 synoptically observing the entire sunlit disk of the Earth (nominal size 0.5^O). EPIC is a 10 wavelength
99 filter camera with a 2048x2048 pixel CCD (charge couple detector) onboard the DSCOVR spacecraft
100 using a 30 cm aperture Cassegrain telescope with a field of view (FOV) of 0.62^O. The sampling size on the
101 Earth is nominally 8 km at the center of the image with an effective spatial resolution of 10x10 km^2 for
102 all 10 filter channels. Operation of EPIC consists of sequentially selecting a filter from 2 rotatable filter
103 wheels and an exposure time using a rotating disk shutter mechanism. Invariant exposure times were
104 set at the beginning of the on-orbit mission to fill the CCD wells to about 80 % and avoid blooming (a
105 saturated pixel affecting its neighbors). The CCD was calibrated for the sensitivity differences between
106 the pixels (flatfielding), and measurements were made in the laboratory and in-flight to obtain
107 corrections for stray light effects. Corrections for dark current are applied based on periodic
108 measurements with the shutter closed. EPIC is kept centered on the Earth during its 6-month north-

109   south tilted Lissajous orbit about the Earth-Sun L_1 point. The spacecraft is never closer than 4° from the
110   Earth-Sun line, which makes it possible to observe an eclipse without the Moon being in the FOV. A
111   more detailed description of EPIC is given in Herman et al. (2018).

112   The geolocated EPIC data (Counts per second, C/s) from each set of 10 wavelengths are
113   contained in an HDF5 formatted file available from the permanent NASA Langley data repository center
114   (https://eosweb.larc.nasa.gov/project/dscovr/dscovr_epic_l1b). Contained in each Level-2 data HDF5
115   file are the 2048 x 2048 array of C/s measured by EPIC and a common latitude and longitude grid. The
116   geolocated data are organized corresponding to the rectangular CCD grid, 1 data point per CCD pixel.
117   For the time of the eclipse, the illuminated CCD pixels are within a circular boundary corresponding to
118    $2.59x10^6$ illuminated pixels (illuminated pixels formed a circle of 1816 pixels in diameter out of a
119   maximum of 2048 pixels. To reduce the volume of data, all measurements, except those from the 443
120   nm channel, were averaged onboard DSCOVR to 1024 x 1024 pixels. After geolocation onto a common
121   latitude x longitude grid, the data from all channels are presented as 2048 x 2048 points with off-earth
122   points represented as a fill value.

Table 1 *Eclipse Measurement Timing and Location Details for 5 Wavelengths*
Eclipse Maximum and EPIC Image Times. Total Measurement Duration 2.7 minutes

Wavelength (nm)	Date and Time	Location Name	Longitude
	2017-08-21 17:35:40	Eclipse West Edge of WY state	$-111^O02'$
551	2017-08-21 17:42:36	West of Casper	$-106^O22'$
680	2017-08-21 17:43:30	West of Casper	$-106^O21'$
Casper Wyoming	2017-08-21 17:43:51	Casper WY	$-106^O19'$
780	2017-08-21 17:44:24	Near Glenrock WY	$-105^O52'$
443	2017-08-21 17:44:50	West of Douglas WY	$-105^O14'$
388	2017-08-21 17:45:18	West of Douglas WY	$-105^O17'$
	2017-08-21 17:48:04	Eclipse East Edge of WY state	$-104^O03'$

123

124   The observing conditions for 21 August 2017 ranged from significant cloud cover over the oceans to
125   nearly clear skies over the United States (Figs. 1 and 2). The synoptic observations provided a unique
126   opportunity to estimate the fraction of reduced reflected radiation from the entire sunlit Earth caused
127   by a total solar eclipse. Two of the synoptic observations were timed so that they centered on Casper,
128   Wyoming (42.8666° N, 106.3131° W, 17:44:50 UTC) and Columbia, Missouri (38.9517° N, 92.3341° W,
129   18:14:50 UTC). Ten narrowband images were obtained at center vacuum wavelengths λ_i of 317.5±0.5,
130   325±0.5, 340±1.3, 388±1.3, 443±1.3, 551±1.5, 680±0.8, 688±0.42, 764±0.5 and 779.5±0.9 nm (Herman
131   et al., 2017). Of these, 388, 443, 552, 680, and 779 nm radiances are not strongly absorbed in the
132   atmosphere and are used for estimating the reduction in reflected radiances from the Earth. The others
133   are strongly affected either by ozone (317, 325, 340 nm) or oxygen absorption (688, 764 nm) in the
134   atmosphere, but give similar eclipse results compared to non-absorbed channels. The non-absorbed
135   wavelength observations were combined to produce eye-realistic color images
136   (https://epic.gsfc.nasa.gov). For this eclipse day study, 21 August, the original color images were
137   modified by increasing the gamma correction to better show the umbra over Casper, Wyoming and

138 Columbia, Missouri (Figs. 1 and 2 based on a suggestion by Steven Albers and Michael Boccara, 2017,
139 Private Communication). The images include Rayleigh scattering effects that cause light from the
140 penumbral region to increase illumination within the umbra along with scattering from clouds and
141 aerosols.

142   Table 1 summarizes eclipse timing and location details for Casper, Wyoming. During the 2.7
143 minutes needed to obtain the five listed wavelength channel images, the center of totality moves at
144 about 46 km/minute or covering approximately 124 km. Based on the image in Fig. 1, the entire
145 measurement took place within the observed almost clear-sky region surrounding Casper, Wyoming.
146 The timing and predicted shape of the Moon's shadow over Casper, Wyoming can be seen at
147 https://eclipse2017.nasa.gov/eclipse-maps. An annotated portion of the figure is reproduced in the
148 Appendix (Fig. A1).

149

150   The predicted totality shadow (Fig. A1) over Casper was elliptical in shape with a width of about
151 116 km (about 1.5^O in latitude or longitude). A similar drawing for Columbia, Missouri shows a more
152 nearly circular region of totality. The dimension of the partial eclipse for 90 % obscuration is about 5° in
153 latitude or longitude. 75 % obscuration covers a latitude range 32° to 46° or about 1200 km. An
154 obscuration region of this size produces a significant decrease in the percentage of total solar irradiance
155 reaching the Earth's surface and in the amount reflected back to space. EPIC synoptically measures both
156 the local and sunlit portion of the global percent change in reflected radiance, which is approximately
157 the same as the percent change in surface irradiance for the wavelength range from 388 to 780 nm. The
158 3 wavelength channels shorter than 388 nm are affected by ozone, and are not included in the
159 quantitative estimate of broadband reduced reflected radiance, nor are the strongly absorbed O_2 A- and
160 B-band channels, 688 and 764 nm, included. However, the effects of the eclipse on all 10 channels are
161 individually estimated.

162

163 **2.1 Monochromatic Eclipse Images**

164

165   Before quantitatively examining the EPIC data from the eclipse in units of C/s or reflectance, the
166 same data can be represented as monochrome grey-scale images. The images (Fig. 3 with North down)
167 range from 340 nm, with strong Rayleigh scattering effects (haze) and some ozone absorption, to 780
168 nm in the near infrared. North is selected as down to correspond to a 3D projection image presented
169 later. Because of the clarity of the atmosphere at 780 nm, the image serves as a geographic map of the
170 Earth as viewed by EPIC where North and South America are clearly visible.
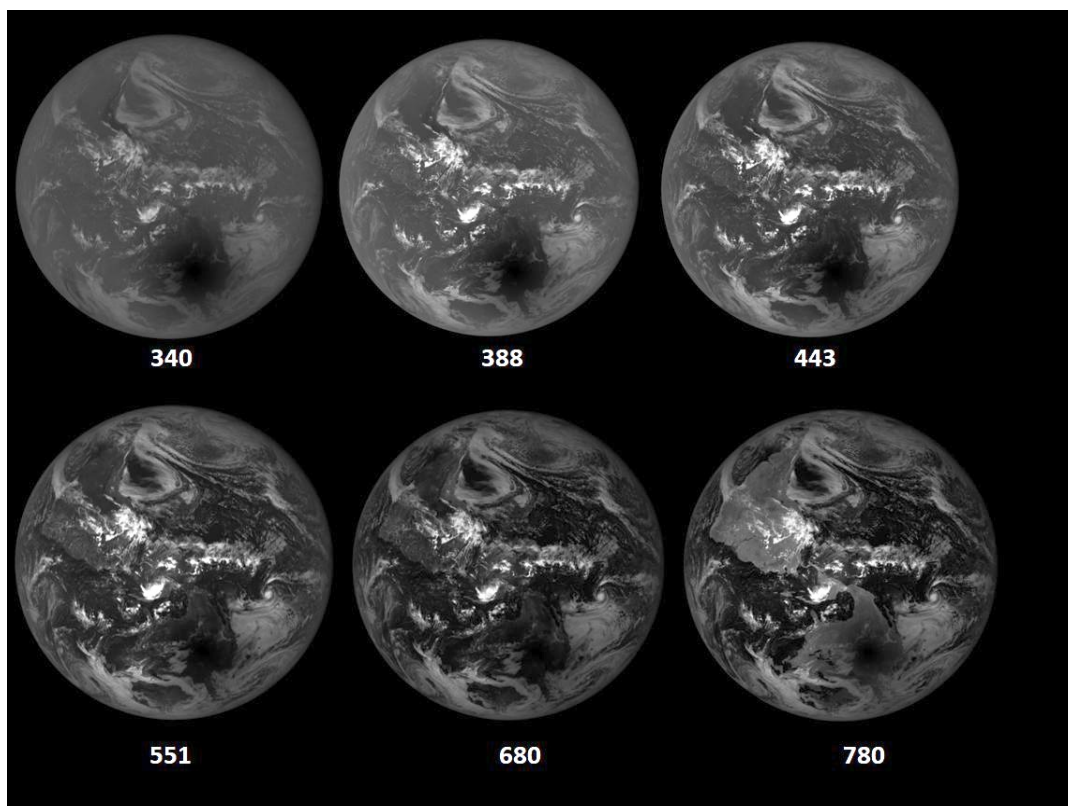
Fig. 3 Greyscale images for 6 of the DSCOVR/EPIC channels for the eclipse over Casper Wyoming showing the blurring caused by Rayleigh scattering and the dark land and ocean surfaces at 340 nm to the almost clear atmosphere and bright continental surfaces at 780 nm. The images were obtained over a period of 2.7 minutes. North is facing down.

171

172 **3.0 Results**

173 **3.1 Comparison of Eclipse and Non-Eclipse Days for Casper, WY and Columbia, MO**

174   Atmospheric conditions during the eclipse at Casper, Wyoming were almost cloud-free

175 compared to Columbia, Missouri, which had optically thin low altitude clouds (Fig. 2). Figure 4 shows the

176 cloud cover on the day of the eclipse, 21 August 2017 (panel A) about 90 minutes before totality at

177 Casper and about 2 hours after totality. The images (north is up) show that the skies remained relatively

178 clear over the northern United States for the duration of the eclipse. A similar set of images (panel B)

179 are shown for the day before (20 August) and two days after the eclipse (23 August). There was no

180 useable data available on 22 August. Data obtained on these days at approximately the same UTC

181 (backscatter phase angle for given location on Earth) as occurred during the total eclipse are used as

182 reference data to compare with the eclipse data. The basic global patterns of cloud cover are similar for

183   all three days, but not identical. As shown later, the amount of light reflected back to space is
184   approximately the same on two non-eclipse days 20 August and 23 August.
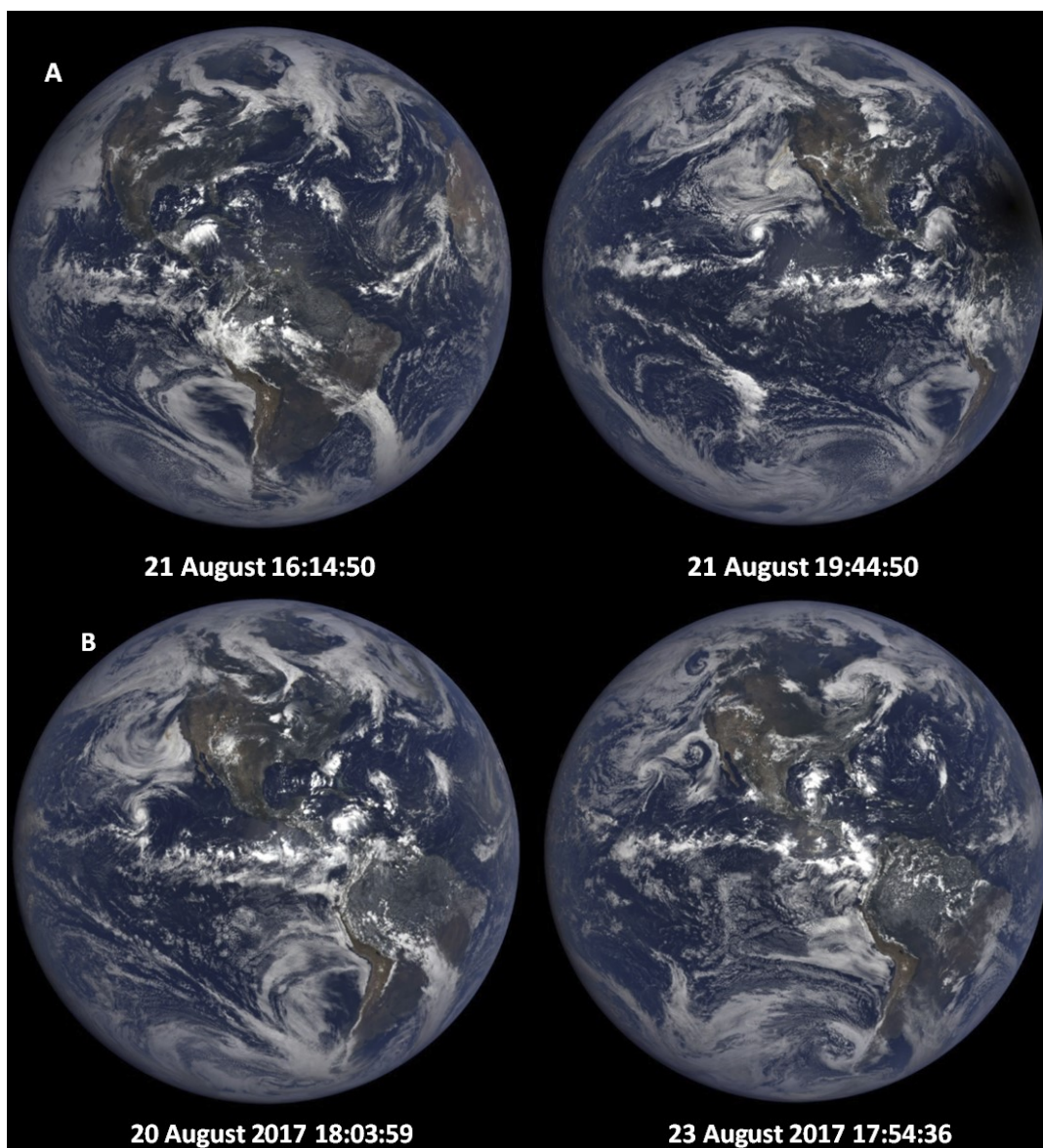
Fig. 4 Panel A: Synoptic natural color images on 21 August at 16:14 and 19:44 before and after the eclipse over the US, and Panel B: the days before and after the eclipse selected to be as close as possible to the phase angle (UTC 17:44:50) as the time of totality over Casper, Wyoming. North is facing up.

185

186   Figure 5 (upper panels A and B) shows longitudinal slices of reflected solar radiances in C/s
187   towards L_1 through the locations corresponding to Casper, Wyoming and Columbia, Missouri at their

188   respective times of totality. The lower panels (C and D) of Fig. 5 show 443 nm measurements in C/s on

189   20 Aug at 18:04 UTC before the eclipse for nearly identical solar phase angles conditions for both sites.
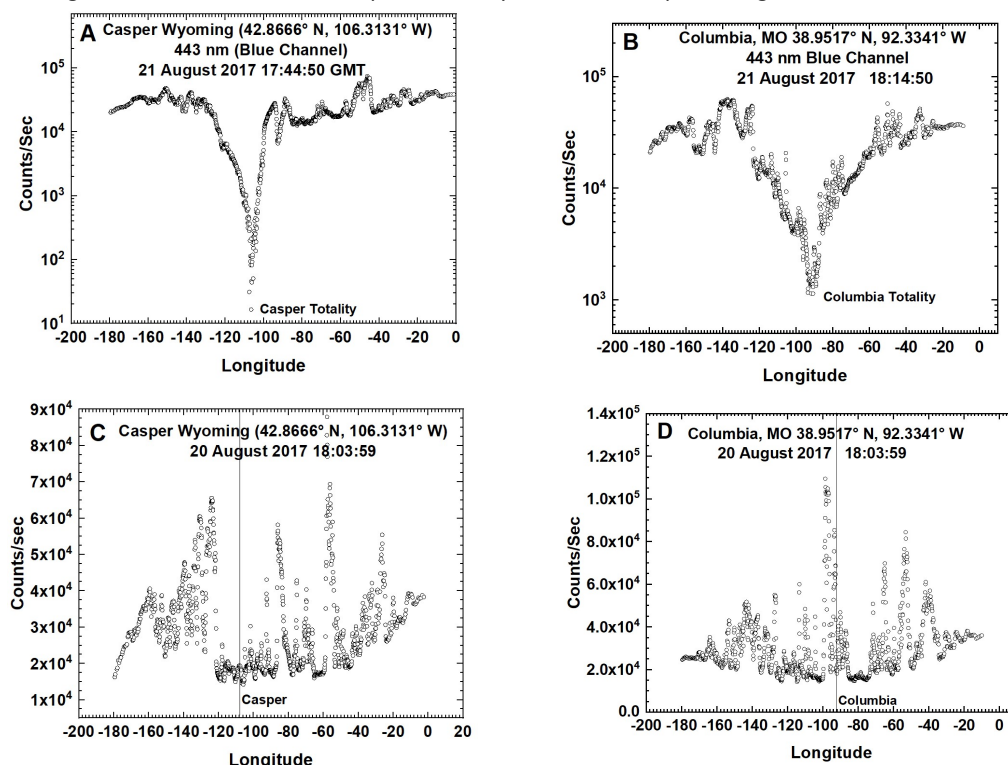
Fig. 5 Top: The effect of an eclipse (21 Aug) on the measured C/s reflected back to space as a function of longitude (degrees) for two locations, Casper Wyoming (left) and Columbia Missouri (right). Middle: Measured C/s reflected back to space on 20 Aug.

190

191   While Fig. 5 is expressed in C/s, the 443 nm data can be converted to radiance $W/(m^2 \text{ nm sr})$

192   based on an in-flight determined calibration coefficient of 5.291×10^{-6} (Geogdzhayev and Marshak, 2017).

193   For the 2.6 nm wide 443 nm channel, an average count rate for the illuminated earth is 3×10^4 C/s

194   corresponding to a radiance of 0.413 $W/(m^2 \text{ sr})$. EPIC calibration constants for 8 of the 10 channels were

195   obtained by in-flight comparisons of reflectance measured by two well calibrated low Earth orbiting

196   satellite instruments, OMPS (Ozone Mapping Profiler Suite) and MODIS (Moderate Resolution Imaging

197   Spectroradiometer) for simultaneously viewed Earth areas with the same satellite view and solar zenith

198   angles (Herman et al., 2018; Geogdzhayev and Marshak, 2017). The O_2 A- and B-band channels were

199   calibrated using lunar data when the Moon was within the field of view of EPIC. Detailed discussions and

200   values of all EPIC calibration coefficients $K(\lambda)$ are given by Geogdzhayev and Marshak (2017), Herman et

201   al, (2018) and Marshak et al., (2018). Most of the conclusions in this study are in terms of ratios of C/s

202   from the same wavelength channel that are independent of the absolute calibration conversion from

203   C/s to radiance.

204
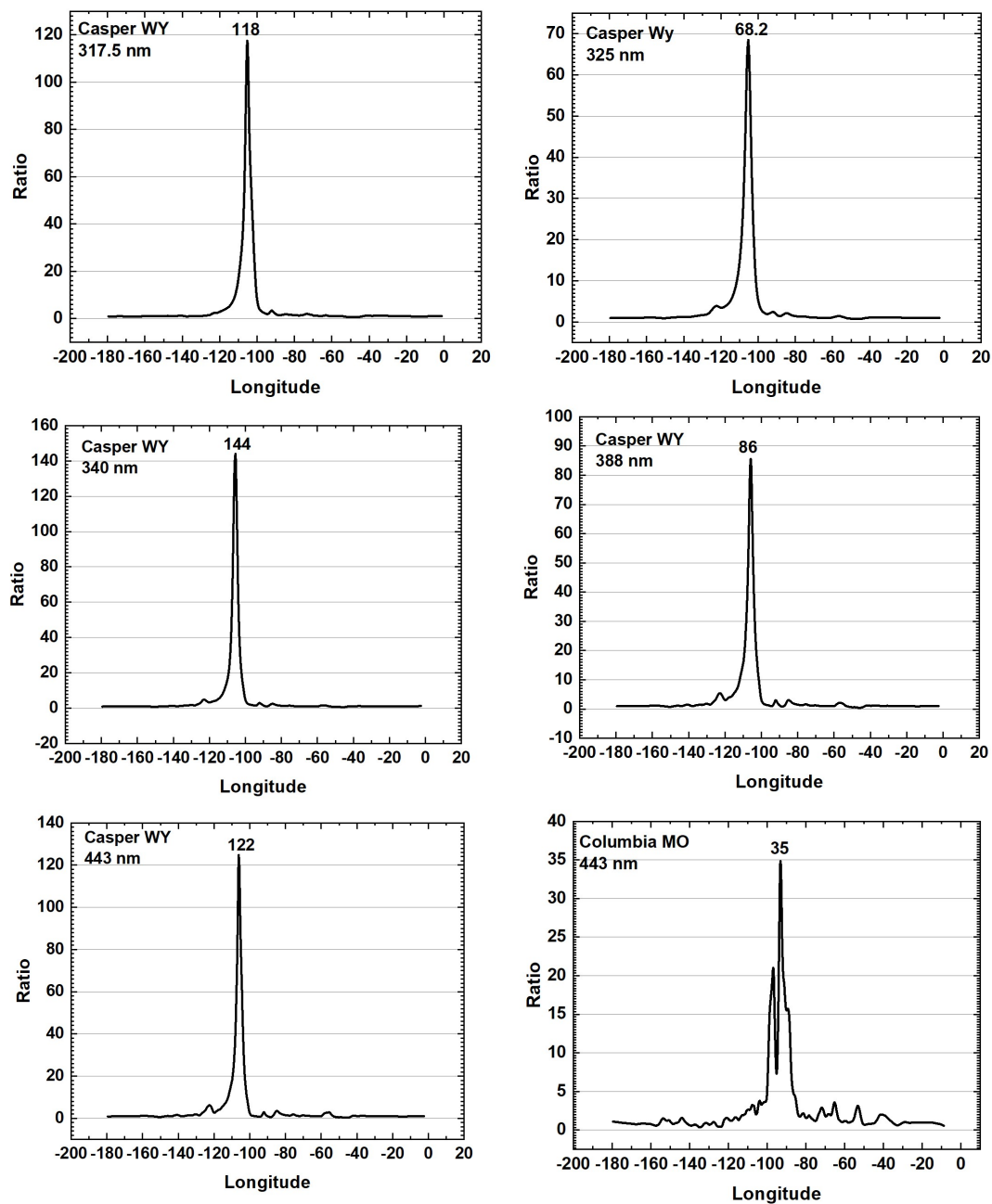
Figure 6a The spatially averaged ratio $\langle R_{EN}(\lambda_i) \rangle = \langle I(Aug20) \rangle / I(Aug21) \rangle$ at the time of the Eclipse in Casper Wyoming for wavelengths 317.5 to 443 nm. For comparison, $\langle I(Aug20) \rangle / \langle I(Aug21) \rangle$ 443 nm for Columbia MO is shown.

205

206
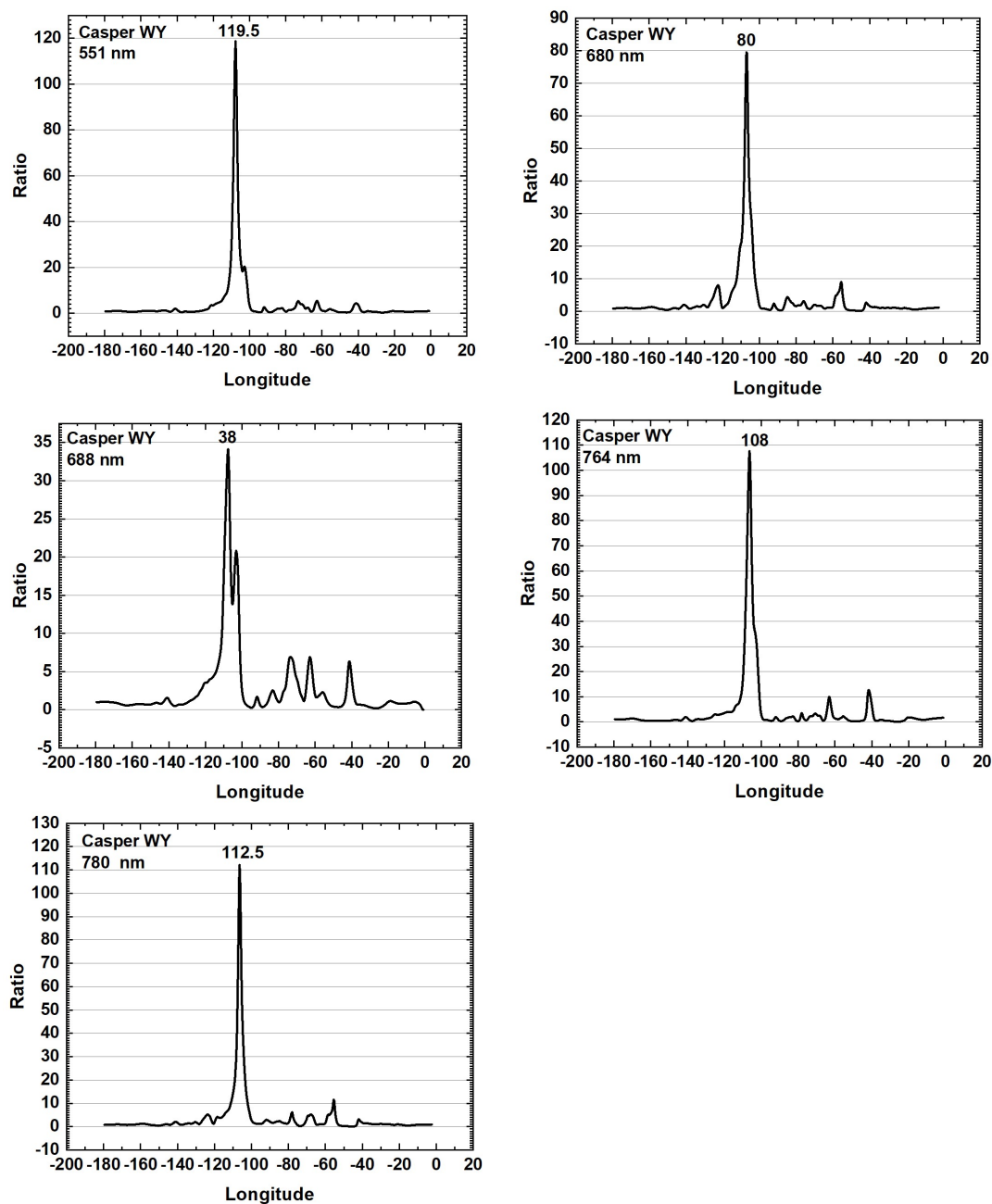
Fig. 6b The spatially averaged ratio $\langle R_{EN}(\lambda_i) \rangle = \langle I(Aug20) \rangle / I(Aug21) \rangle$ at the time of the Eclipse in Casper Wyoming for wavelengths 551 to 780 nm. The channels 688 and 764 nm are within the O_2 B and A absorption bands

208   Because of the spatial variability in C/s on both 20 Aug. and 21 Aug. the C/s data were smoothed
209   (spatially averaged) using a Lowess(0.025) fit (Locally Weighted least squares fit to 0.025 of the data
210   points, (Cleveland, 1981), or about 30 points). The Lowess(0.025) fit minimizes the effect of possible
211   outlier points compared to a simpler running average. There is considerable variability in $R_{EN}(\lambda_i)$ as a
212   function of wavelength that is partially caused by the 2.7 minutes needed to obtain measurements for
213   all 10 wavelengths. During the 2.7 minutes, the center of totality moved about 124 km or about 1.3^O
214   longitude, meaning that the ratio was affected by atmospheric variability (mostly cloud effects) in the
215   successive scenes containing the eclipse totality for each wavelength. The spatially averaged (indicated
216   by <>) ratio $<R_{EN}(\lambda_i)>$ = <I(20 August)>/<I(21 August)> of C/s on the eclipse day to the preceding non-
217   eclipse day is shown in Fig. 6 for all 10 wavelength λ_i channels and summarized in Table 2.

218

Table 2 Maximum Radiance Ratio $<R_{EN}(\lambda_i)>$ during eclipse totality 17:45 UTC compared to 20 Aug

219

Wavelength λ_i (nm)	Max. $<R_{EN}(\lambda_i)>$ C/s
317.5	118
325	68.2
340	144
388	86
443	122
551	119.5
680	80
688	38
764	108
780	112.5

226   For the eclipse study, the range of synoptically observed longitudes is approximately from the
227   international dateline (-180°) to approximately the longitude of Greenwich, England (0°). The nearly
228   clear-sky in Casper with optically thin high cirrus clouds allowing the reflected light during totality to
229   become very small (about 50 C/s for 443 nm compared to 1.7×10^4 C/s on 20 August at the same
230   longitude). Columbia had more low altitude cloud cover than Casper (Fig. 2) with the cloud cover
231   extending into the region of totality. The effect of this cloud cover can be seen in Fig. 6a (lower right
232   panel), where the maximum $<R_{EN}(443, Columbia)>$ = 35 compare to 122 for Casper. Table 2 provides the
233   eclipse radiance ratio $<R_{EN}(\lambda_i)>$ for the five non-absorbed wavelength and 5-absorbed channels that can
234   help validate 3D radiative transfer models. A detailed radiative transfer study for realistic conditions is
235   made feasible by using EPIC's simultaneous estimates of cloud reflectivity and transmission, cloud
236   height, aerosol amounts, and ozone amounts.

237   A 3D Monte Carlo radiative transfer calculation obtained a non-eclipse to eclipse irradiance ratio
238   at 340 nm (Emde and Mayer, 2007) for clear-sky conditions applicable to the similar overhead geometry
239   of the 29 March 2006 eclipse. The ratio was a factor of 1.7×10^4 at 340 nm and was estimated to be
240   higher for longer wavelengths. The results before spatial averaging (similar to Fig. 5) from the present
241   study are $R_{EN}(340\ nm)$ = 515±27, which suggest that 1.7×10^4 is too high under realistic atmospheric
242   conditions. The lower values of spatially averaged $<R_{EN}(\lambda_i)>$ show that there is high sensitivity of the

243   measured ratios to the presence of even optically thin clouds.   Broadband measurements and
244   meteorological model studies during the eclipse of 29 March 2006 near the Athens, Greece city center
245   showed a ratio of about 800 from the near-noon values prior to the 84 % eclipse (Psiloglou and
246   Kambezidis, 2007). The broadband study showed a reduction total solar irradiance in the presence of
247   light clouds. The light clouds were indicated by the time dependence for the measured solar radiation
248   on 29 March compared with similar measurements on a nearly clear-sky day on 28 March. Radiative
249   transfer model studies (Wen et al., 2008) show that boundary layer clouds can enhance the effect of
250   Rayleigh scattering into clear-sky regions. For the region of geometrical eclipse totality, the combined
251   cloud and molecular scattering mechanisms are important contributors to the amount of radiation
252   transmitted to the ground and reflected back to space.

254   **3.2 Global reduction of reflected sunlight during the eclipse over Casper WY**

256   The unique DSCOVR/EPIC measurements provide estimates of the fractional reduction of
257   sunlight from 388 to 780 nm reflected back to space for the entire sunlit globe caused by the eclipse
258   shadow on the Earth. To do this, all of the light reaching EPIC in each of the five non-absorbed channels,
259   388, 443, 551, 680, and 780 nm, are integrated over the visible sunlit Earth and compared (percent
260   difference PD) with a nearly identical viewing geometry (nearly the same UTC) from the previous and
261   next days. The assumption is that the major cloud features change slowly on a global scale over
262   relatively short periods (Figs. 1 to 3). A test of this hypothesis is that the PD between successive non-
263   eclipse days is small compared to the eclipse day PD with a non-eclipse day.

264   In the 3D Fig. 7 for 443 nm, the nearly cloud free eclipse region is the blue area in the midst of
265   greens, yellows, and reds. The high red values correspond to fairly reflective clouds mostly seen near
266   the equator (Fig. 1). The yellows and greens correspond to lower altitude clouds that tend to have
267   smaller reflectivities. Integrating over all of the pixels for the eclipse on 21 August 2017, using the file
268   named epic_1b_20170821174450_02.h5, we get S(DOY, UTC) = 5.34366×10^{10} C/s for DOY=233 (21
269   August 2017) and UTC=17:44:50. The average C/s = 2.0631×10^4, which corresponds to 0.89 W/m^2.
270   Peak values are approximately 1×10^5 C/s, or about 4.3 W/m^2. Figure 7 is oriented with north down so
271   as to be able to see into the eclipse shadow region.

272   The EPIC file name from the NASA archive is interpreted as Year 2017, Month 08, Day 21, UTC
273   17:44:50, Version 2, which is 11:44:50 local daylight savings time in Casper, Wyoming. The filename time
274   refers to approximately the middle of the measurement sequence. Totality in Casper started at 11:42:39
275   and ended at 11:45:05. Version 2 refers to the reprocessing of data with the latest CCD flat-fielding and
276   stray-light corrections (Herman et al., 2017; Marshak et al., 2017; Geogdzhayev and Marshak, 2017), and
277   the geolocation algorithms that puts all 10 of the wavelength measurements on a common latitude by
278   longitude grid.

279   Measured C/s images for six wavelength channels (340 to 780 nm) on 20, 21, and 23 August (Fig.

280   8) were selected to be as close as possible to the UTC time of the eclipse in Casper Wyoming, keeping

281   the scattering phase angles nearly constant. Similar images for the 317.5, 325, 688, 764 nm channels are

282   shown in the appendix (Fig. A2). The middle images in panels B and E of Figs. 8a, 8b and 8c are for the

283   eclipse over Casper, Wyoming. These images are in the same format as Fig. 3, but rotated with north up.

284   Unlike Fig. 3, The scale in Fig. 8 was selected so that the brightest clouds do not saturate the image. The

285   increase in scale makes the land surfaces less visible. While the figures are similar from wavelength to

286   wavelength, there are differences in the depth of the eclipse totality and the reflectivities of the

287   surrounding clouds.
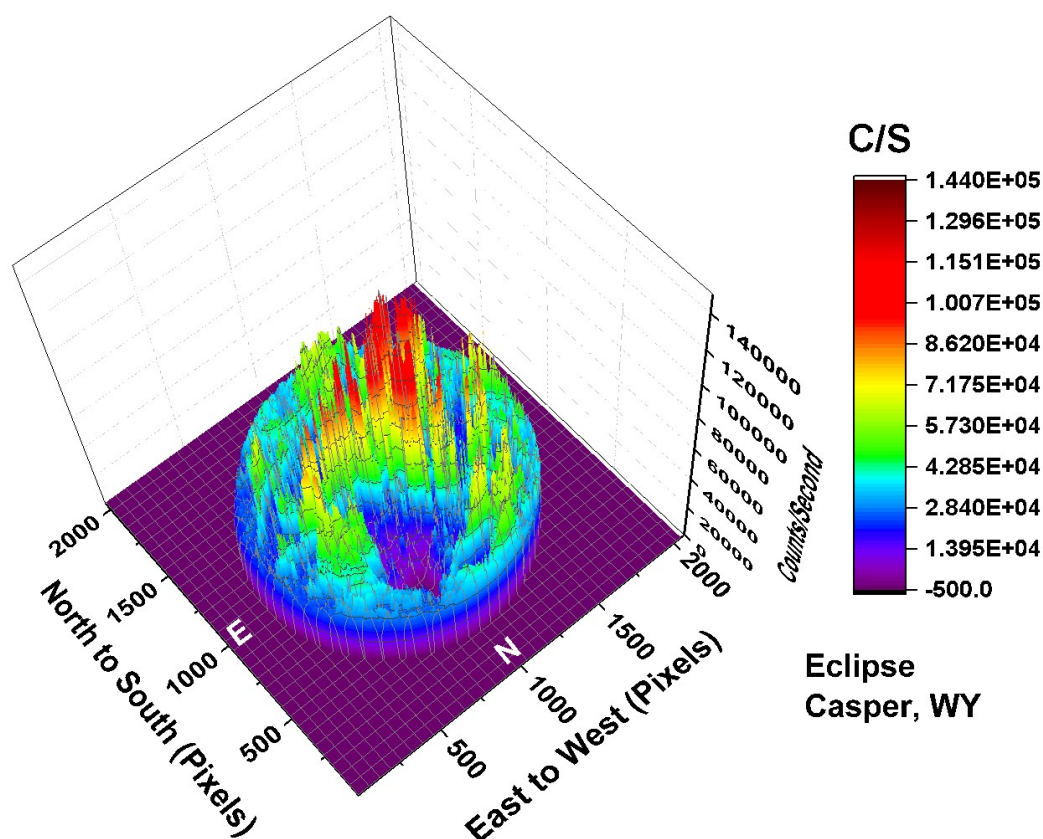
Fig. 7 The C/s observed by EPIC for the 443 nm channel corresponding to the color image shown in Fig. 1. In the data file, the word infinity has been replaced by the number zero. In this image there are approximately 2.59×10^6 illuminated pixels out of $2048^2 = 4.194304 \times 10^6$ pixels (61.8 %).

288

289

290

Table 3 Eclipse change in reflected light at Casper, WY from 20, 21, 23 August 2017 Units are ICs x 10^{-7}

λ_i (nm)	20 August 2017 16:58:31	21 August 2017 17:44:50	23 August 2017 17:54:36	Avg. PD
317.5	280.5	258.8	282.0	9±0.41
325	460.6	425.5	464.2	9±0.59
340	3183	2946	3213	9±0.72
388	2034	1878	2044	9±0.37
443	5808	5344	5813	9±0.066
551	5619	5078	5573	10±0.64
680	3790	3433	3773	10±0.35
688	1129	1010	1110	11±1.3
764	671.9	585.9	651.9	13±2.4
780	2794	2491	2999	16±5.8

291

292   Figure 8 can be converted from counts/second $C(\lambda)$ to reflectance $Re(\lambda)$ using the in-flight
293   derived calibration coefficients $K(\lambda)$, where $Re(\lambda) = K(\lambda) C(\lambda)$. For the six wavelength channels in Fig. 8,
294     $K(340) = 1.975E-05$, $K(388) = 2.685 \times 10^{-05}$, $K(443) = 8.340 \times 10^{-06}$, $K(551) = 6.660 \times 10^{-06}$, $K(680) =$
295   9.300×10^{-06}, and $K(780) = 1.435 \times 10^{-05}$. To estimate the percent reduction in outgoing radiances, the
296   ratios of integrals over the illuminated CCD (Fig. 8) for each wavelength channel are formed for nearly
297   the same Earth geometry on days preceding and following the eclipse so that either the integrated
298   reflectances or the integrated C/s x 10^{-7} (Table 3) over the CCD pixels, $ICs(\lambda)$, can be used directly, since
299   they are linearly proportional to the integral of the photons received by the illuminated pixels.

300   For the 443 nm channel, the result is an approximate decrease of 9 % on 21 August at 11:44:50
301   local time. As a reference, we compare two non-eclipse days (19 and 23 August). The relative difference
302   is (5860-5813)/5813 < 0.1 %, which is much smaller than the 9 % decrease produced by the eclipse on 21
303   August. The results are summarized for all ten wavelength channels in Table 3. The comparison between
304   two non-eclipse days gives a measure of the uncertainty in the calculation (e.g., 9 ± 0.07 %).

305

306   Percent difference $PD(\lambda_i)$ calculations for λ_i = 317.5, 325, 340, 388, 443, 551, 680, 688, 764, and
307   780 nm, based on a 2-dimensional integration for C/s are summarized in Table 3, yielding $PD(\lambda_i)$ = 9, 9,
308   9, 10, 10, 11, 13 and 16 % reductions in backscattered radiances in the direction of L_1, respectively. The
309   Avg. PD(764) within the strongly absorbing O_2 A-band is 13 %, even though the reflected $ICs(768)$ is
310   much lower than the surrounding non-absorbed bands. $PD(\lambda_i)$ is smaller at shorter wavelengths because
311   of increased Rayleigh scattering that reduces the contrast of the Moon's shadow by scattering light into
312   the totality region from the adjacent area of the partial eclipse. The fact that adjacent absorbed and
313   non-absorbed wavelengths give consistent $PD(\lambda_i)$ suggests that most of the effect comes from clouds
314   and Rayleigh scattering and not from the relatively low reflectivity surface where the amount of clear-
315   sky penetrating radiances are small for 688 and 764 nm channels.

316

317
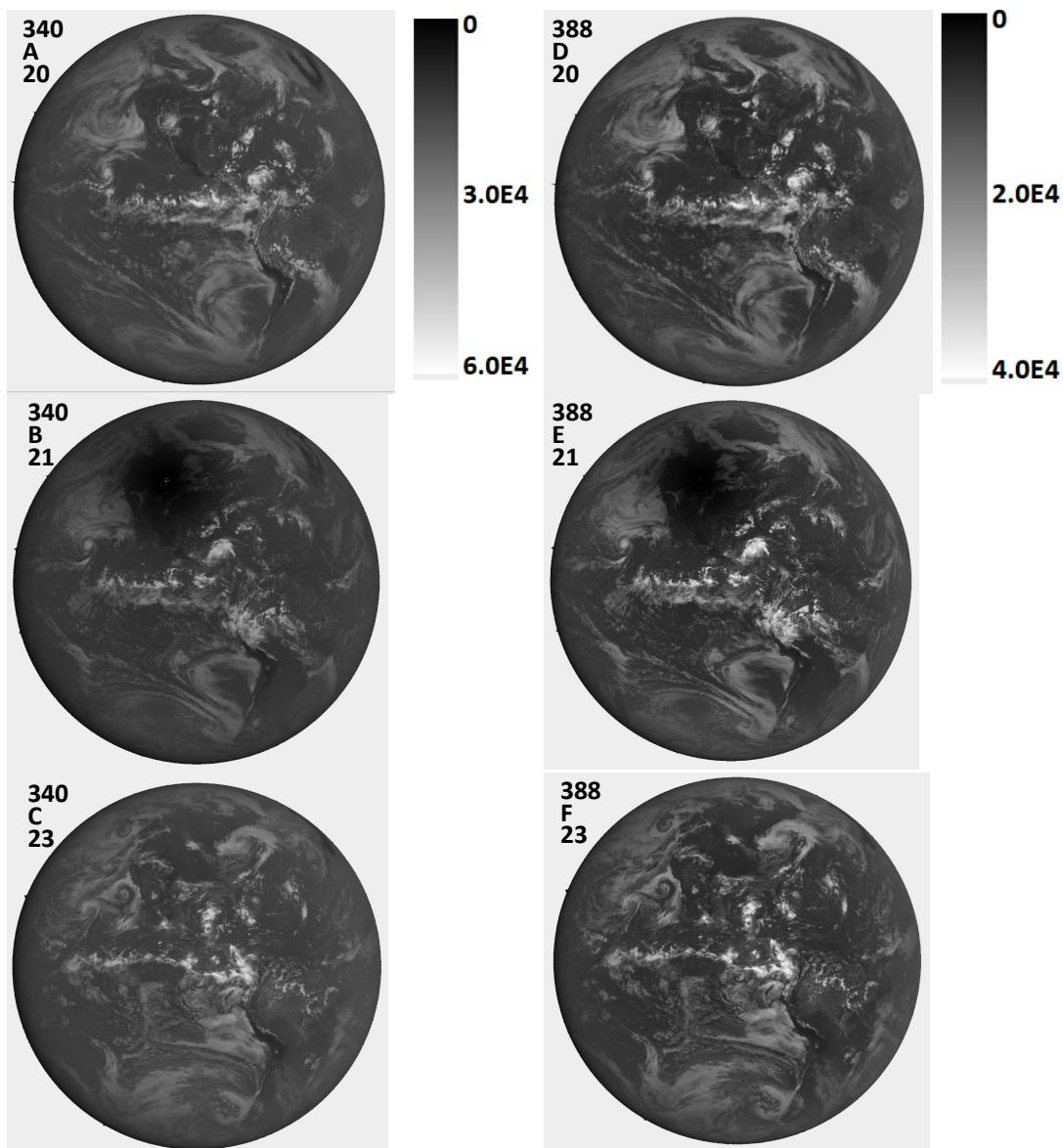
Figure 8a Image in C/s for 340 and 388 nm for 20 Aug.(A+C), 21 Aug. (B+E), and 23 Aug. (C+F). The scale applies to the specific wavelength. North is up.

318

319
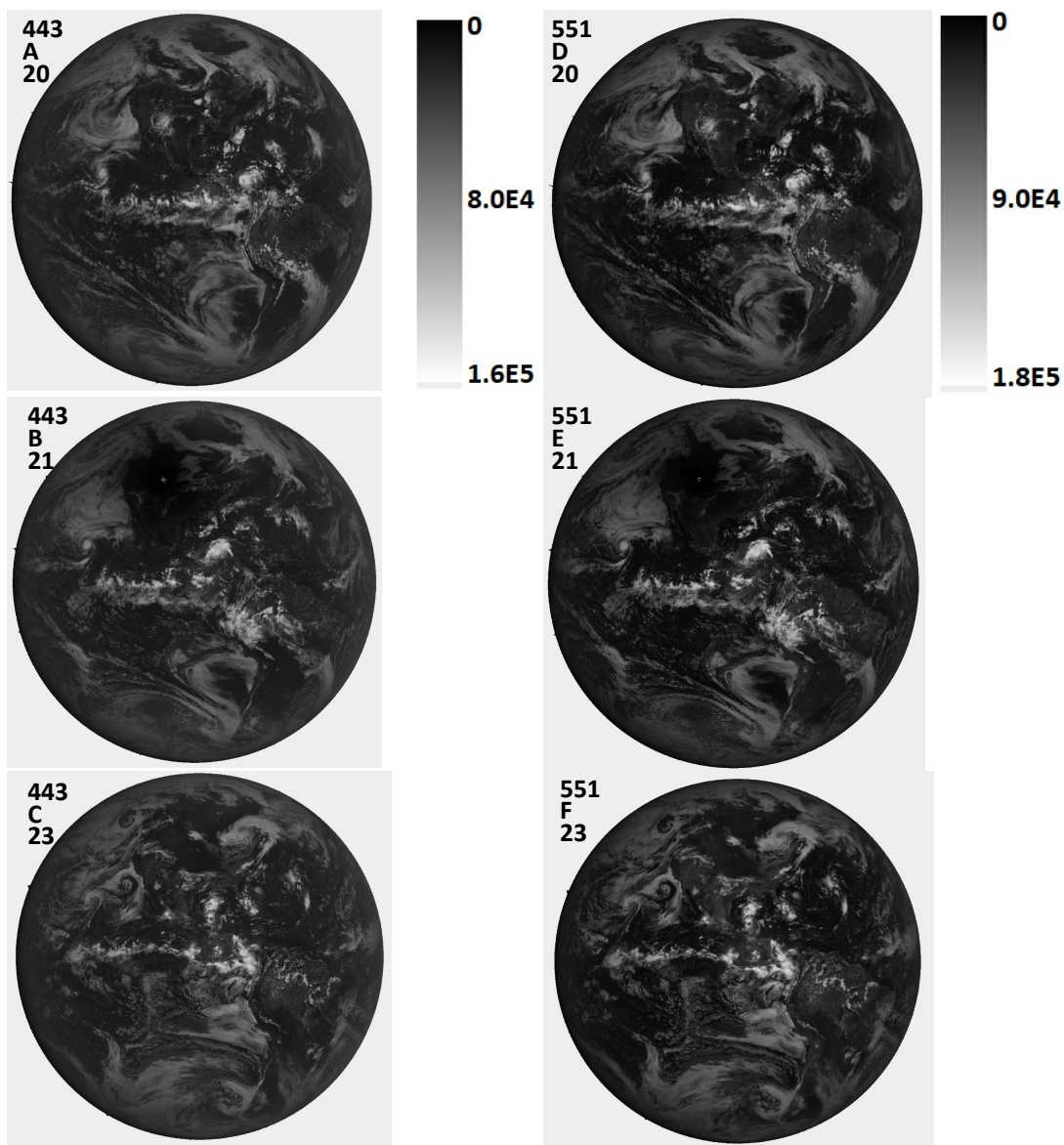
Figure 8b Image in C/s for 443 and 551 nm for 20 Aug.(A+C), 21 Aug. (B+E), and 23 Aug. (C+F). The scale applies to the specific wavelength. North is up.

320

321
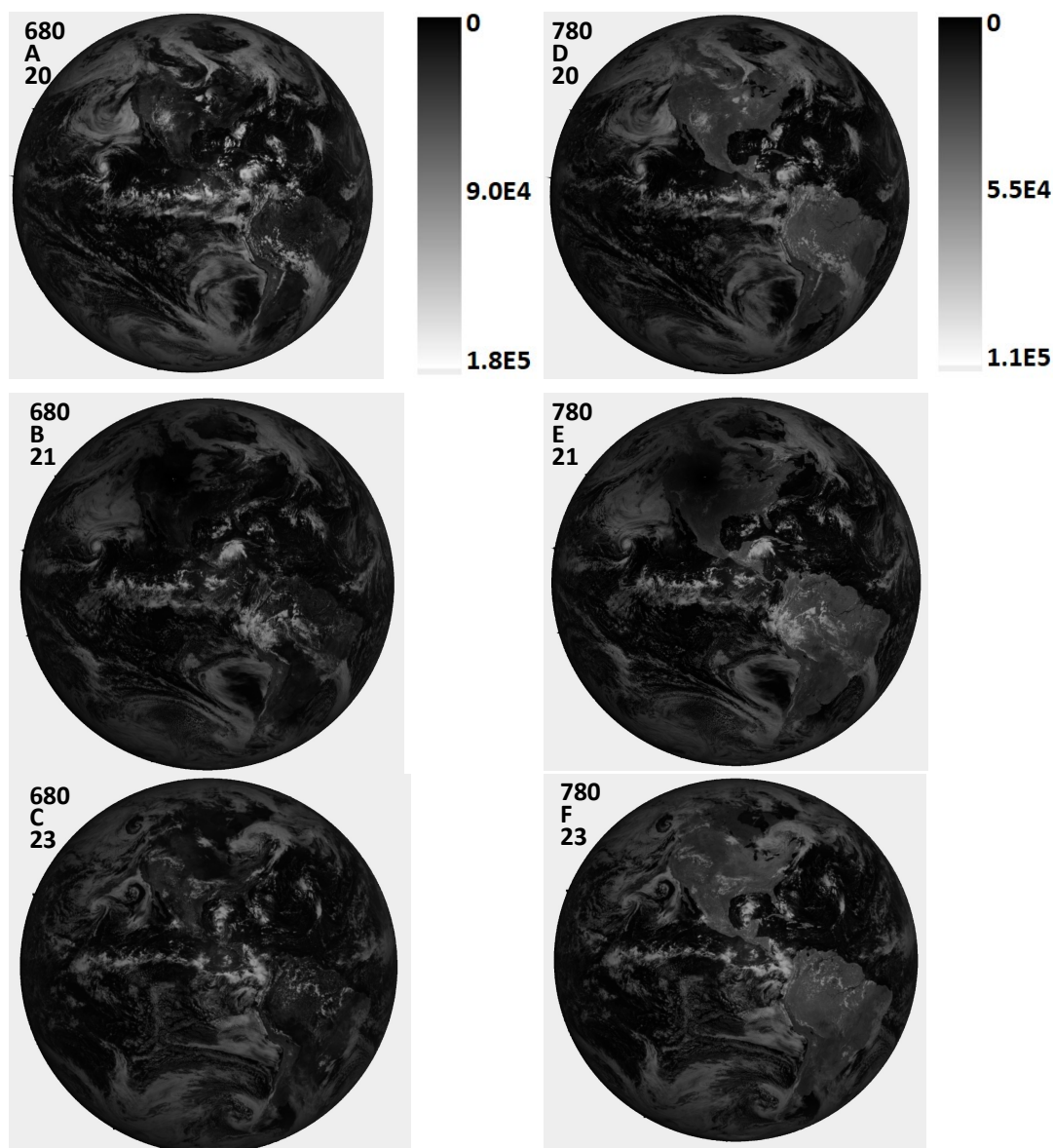
Figure 8c Image in C/s for 680 and 780 nm for 20 Aug.(A+C), 21 Aug. (B+E), and 23 Aug. (C+F). The scale applies to the specific wavelength. North is up.

322

323   The eclipse measurements made by EPIC are near the backscatter direction (172°) for the
324 incident solar irradiance over nearly cloud-free scenes. This means that EPiC is observing close to
325 "hotspot" conditions where the backscatter amount increases with increasing wavelength (Maignan et
326 al., 2004). At 551 and 680 nm the hotspot effect is smaller than at 780 nm.

327

328   To estimate the fractional reflected radiance reduction for the wavelength range from 388 to
329   780 nm, a polynomial interpolation $R(\lambda)$ of the Avg. PD in Table 3 for the 5 weakly absorbed channels is
330   formed (Fig. 9a) that must be weighted by the solar irradiance spectrum $F(\lambda)$. The solar spectrum used is
331   a combination of measured solar flux data named atlas_plus_modtran (Mayer and Kylling, 2005). The
332   components, F_R and F_S, of the weighted average <R> are defined in Eqns. 1 and 2. On 21 August 2017 the
333   distance of the Earth from the Sun was 1.011 AU, or F_S(21 Aug) = 689.98 W/m^2 and F_R = 67.05 W/m^2. F_S
334   is about half of the total solar irradiance of 1361 W/m^2 at the top of the atmosphere at 1 AU (Kopp and
335   Lean, 2011), where

336

$$F_S = \int_{387}^{781} F(\lambda)d\lambda \qquad F_R = \int_{387}^{781} R(\lambda)F(\lambda)d\lambda \tag{1}$$

$$<R> = \frac{\int_{387}^{781} R(\lambda)F(\lambda)d\lambda}{\int_{387}^{781} F(\lambda)d\lambda} = 0.097 \tag{2}$$

337
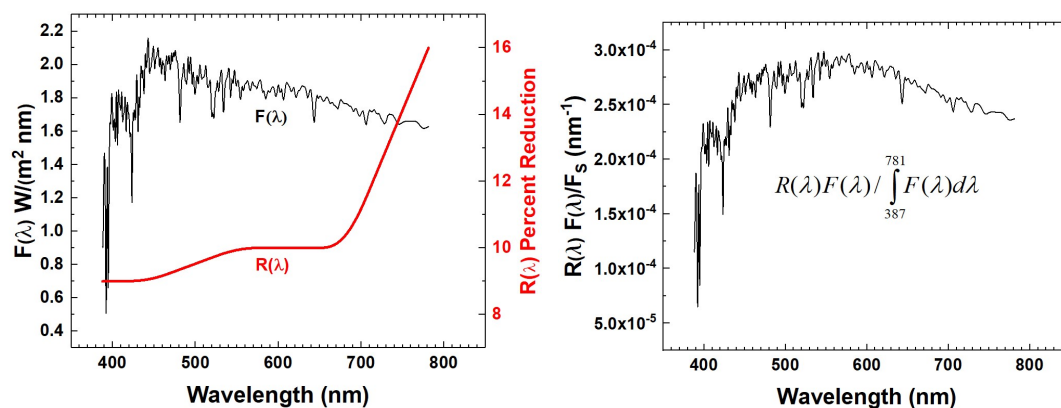
Fig. 9a Solar Irradiance at 1 AU $F(\lambda)$ Watts/(m^2 nm) (Mayer and Kylling, 2005) and the eclipse reduction function $R(\lambda)$ in percent for Casper, Wyoming (red curve).

Fig. 9b Fractional reduction (nm^{-1}) in reflected solar irradiance in the direction of L-1 for Casper, Wyoming.

338

339   Figure 9b shows the product $R(\lambda)F(\lambda)$ /F_S (nm^{-1}). Forming <R> shows that during the eclipse the
340   shadow of the Moon reduces the backscattered radiance (388 to 780 nm) in the direction of L_1 by
341   9.7±1.7 %. The uncertainty ±1.7 % is caused by variations in the cloud cover of the reference days
342   compared the eclipse day. The calculation of <R> is based on C/s measurements from DSCOVR/EPIC of

343   the sunlit Earth and the interpolation function R(λ). The result is independent of the absolute calibration
344   of EPIC, since it is based on ratios of C/s over three days with approximately the same UTC (scattering
345   phase angles). R(λ) includes the near backscatter direction enhanced reflection function appropriate for
346   the entire sunlit disk. The three days at nearly the same UTC can be compared directly, since EPIC has
347   proven to be very stable based on repeated in-flight calibrations over a 2-year period using OMPS and
348   MODIS (Herman et al., 2017 and Marshak et al., 2017). The smooth function R(λ) does not include
349   absorption features from water and the O_2 A- and B-bands.

350   **3.0 Summary**

351   The EPIC instrument onboard the DSCOVR spacecraft synoptically observes the entire sunlit
352   portion of the Earth from an orbit near the Earth-Sun Lagrange-1 point. On 21 August 2017, EPIC was
353   able to observe the totality shadow from the lunar eclipse of the Sun with the Earth's surface for about 3
354   hours (seven 10-channel measurements) as it crossed the United States from west to east (about 1.5
355   hours). When the region of totality was over Casper, Wyoming at 17:44:50 UTC, the reflected 443 nm
356   radiance was reduced to 76 C/s (0.001) W/m^{2}sr in the narrow region of totality. About 30 minutes later
357   the shadow passed over Columbia, Missouri, but the presence of thin clouds in the vicinity of Columbia
358   caused increased reflected radiance to 1145 C/s (0.016 W/m^{2}sr) during totality compared to Casper.
359   The spatially averaged ratio $<R_{EN}(\lambda_i)>$ of reflected radiances within the eclipse totality to radiances for
360   the same geometry on adjacent non-eclipse days was measured for all 10 wavelength channels. The
361   measured $<R_{EN}(443 nm)>$ was smaller for Columbia (71) than for Casper (936), showing the sensitivity of
362   increased cloud cover over Columbia. $<R_{EN}(\lambda_i)>$ forms a useful test of 3-D radiative transfer models for
363   an eclipse in the presence of optically thin clouds. A previously published clear-sky model result for a
364   nearly overhead eclipse ratios and an ocean surface albedo of 0.06 (Emde and Mayer, 2007) had
365    $R_{EN}(340nm)=1.7\times10^4$ compared to the measured non-averaged $R_{EN}(340)$ at Casper of 515±27 with
366   optically thin clouds under similar geometrical conditions. The measured radiance ratios $R_{EN}(\lambda_i)$ can
367   serve as a validation data set for 3D radiative transfer models of the atmosphere that include cloud
368   effects, since EPIC also measures the surrounding amount of cloud cover for the entire sunlit Earth.
369   Under almost clear-sky conditions, Rayleigh scattering combined with low optical depth clouds also can
370   scatter light into the umbra region and reduce $<R_{EN}(\lambda)>$. Outside of the region of totality, EPIC observed
371   the partial eclipse shadow and the fully illuminated regions of the Earth's disk. Interpolating between
372   the percent reductions $<R_{EN}(\lambda_i)>$ for the 5 measured wavelength channels showed that the integrated
373   reflected radiance from the Earth's sunlit disk towards L_1 decreased by about 9.7 % compared to the
374   average radiances measured on the days before and after the eclipse for approximately the same
375   observing geometry as occurred during the eclipse. Similar calculations comparing two non-eclipse days
376   show smaller changes (0.1 %) than the eclipse-day change. The five channels that are partially absorbed
377   in the atmosphere give consistent results compared to the non-absorbed channels suggesting that cloud
378   reflectivities dominate the 317.5 to 780 nm radiances reflected back to space from the sunlit Earth's disk
379   with a contribution from Rayleigh scattering for the shorter wavelengths.

380

Appendix

The course of the eclipse in the vicinity of Casper Wyoming is shown in Fig. A1
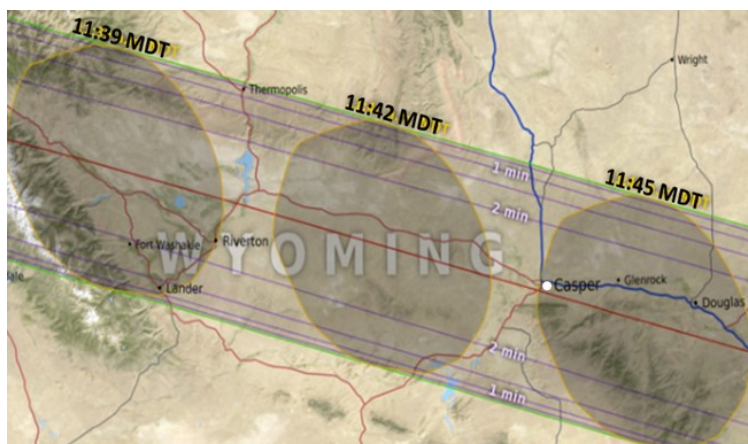
Fig. A1 The timing and shape of the Moon's shadow over Casper, Wyoming showing the relative location of Casper (white circle) at 11:45 MDT (Mountain Daylight Time). The shadow is moving at about 46 km/minute. (https://eclipse2017.nasa.gov/eclipse-maps).

Greyscale images for the four wavelength channels (317.5, 325, 688, 764 nm) whose radiances are strongly absorbed in the atmosphere are shown in Figs. A2a and A2b
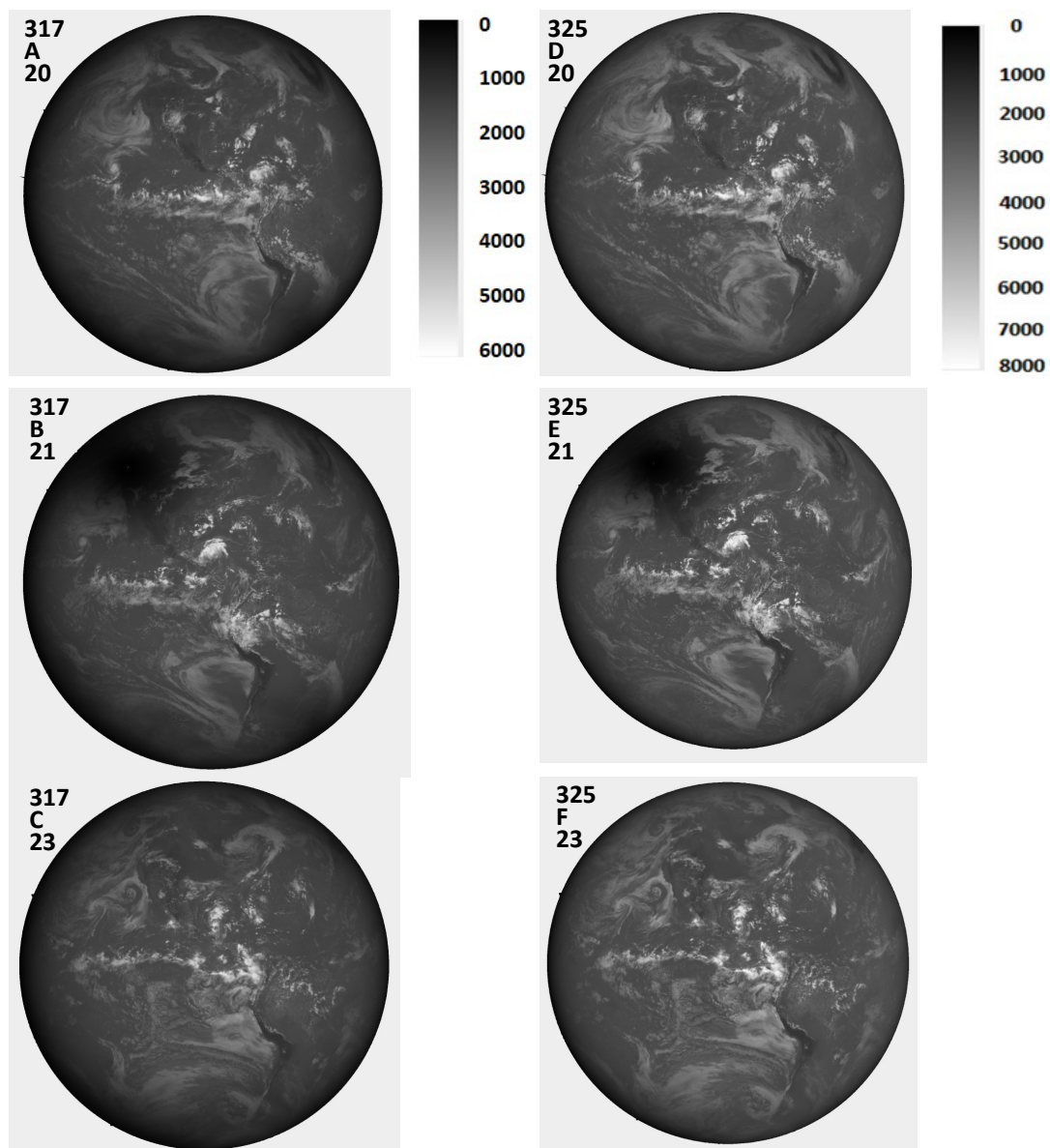
Fig. A2a Image in C/s for 317 and 340 nm for 20 Aug., 21 Aug. and 23 Aug. The scale applies to the specific wavelength. North is up.
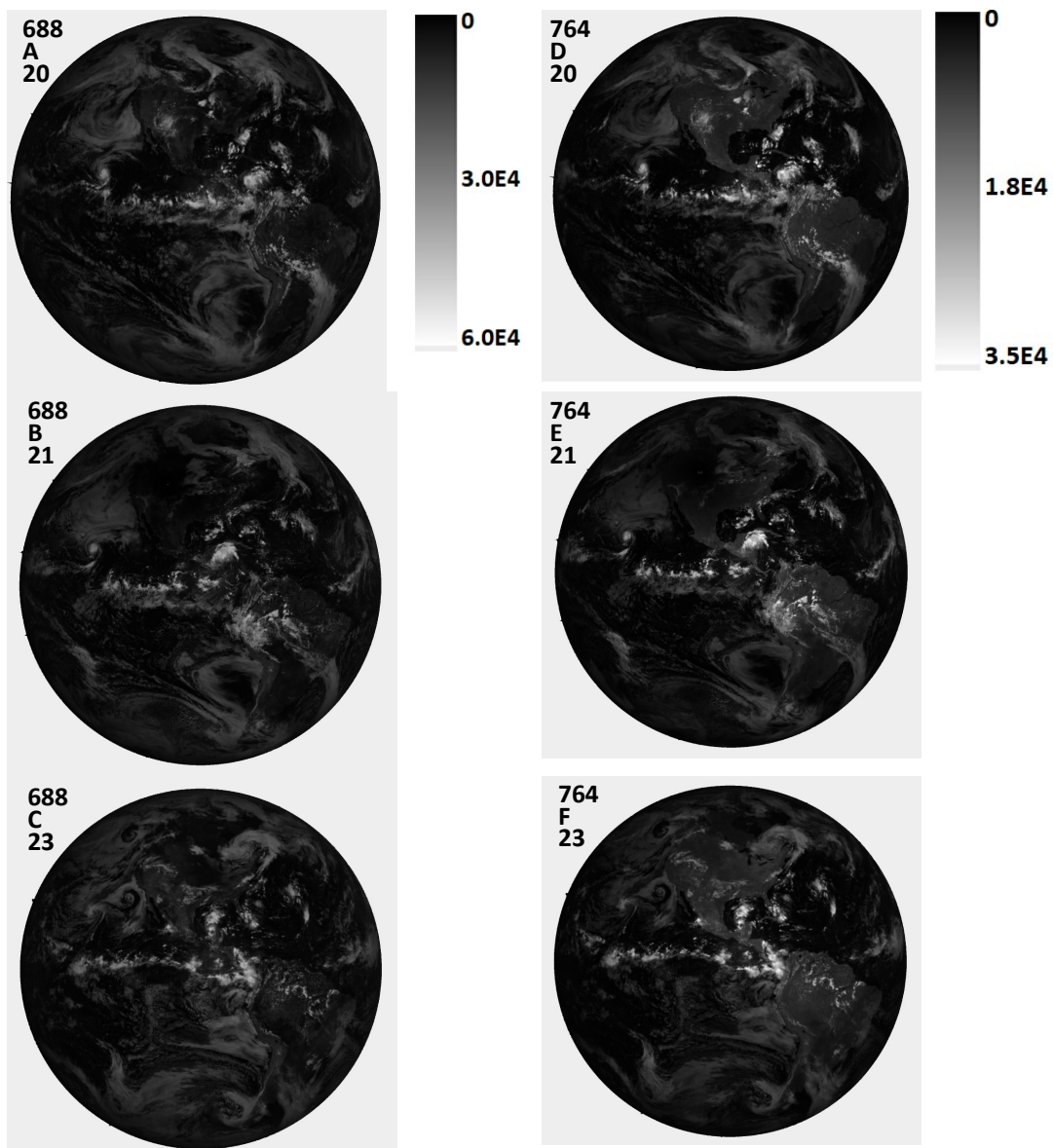
Fig. A2b Image in C/s for 688 and 764 nm for 20 Aug., 21 Aug. and 23 Aug. The scale applies to the specific wavelength. North is up.

389

390

391

392

393 **4.0 Author Contributions**

394 Jay Herman wrote most of the paper and performed most of the calculations

395 Guoyong Wen is the funded principal investigator of the project.

396 Alexander Marshak provided the calibration coefficients for the visible and near-IR channels

397 Karin Blank provided the color images in Figs. 1 to 3. She was responsible for the geolocation of the 10

398 filter images on a common grid.

399 Liang Huang provided the calibration coefficients for the UV channels

400 Alexander Cede provided the flatfielding, stray light correction, and dark current analysis

401 Nader Abuhassan helped with flatfielding and stray light correction and was responsible for the ground-

402 based portion of this research.

403 Matthew Kowalewski provided the flatfielding, stray light correction, and dark current analysis

404

405

406 The authors declare that they have no conflict of interest.

5.0 References

Cleveland, William S., LOWESS: A program for smoothing scatterplots by robust locally weighted regression. The American Statistician. **35** (1): 54. JSTOR 2683591. doi:10.2307/2683591, 1981.

Emde, C. and B. Mayer, Simulation of solar radiation during a total eclipse: a challenge for radiative transfer,(2007) Atmos. Chem. Phys., 7, 2259–2270.

Geogdzhayev, Igor V. and Alexander Marshak, (2017) Calibration of the DSCOVR EPIC visible and NIR channels using MODIS and EPIC lunar observations, Atmos. Meas. Tech. Discuss., https://doi.org/10.5194/amt-2017-222.

Gerasopoulos, E., Zerefos, C. S., Tsagouri, I., Founda, D., Amiridis, V., Bais, A. F., Belehaki, A., Christou, N., Economou, G., Kanakidou, M., Karamanos, A., Petrakis, M., and Zanis, P.: The total solar eclipse of March 2006: overview, Atmos. Chem. Phys., 8, 5205-5220, https://doi.org/10.5194/acp-8-5205-2008, 2008.

Herman, J.R., Alexander Cede, Elena Spinei, George Mount, Maria Tzortziou, Nader Abuhassan, (2009) NO_2 Column Amounts from Ground-based Pandora and MFDOAS Spectrometers using the Direct-Sun DOAS Technique: Intercomparisons and Application to OMI Validation, J. Geophys. Res., 114, D13307, doi:10.1029/2009JD011848, 2009.

Herman, J.R., R.D. Evans, A. Cede, N.K. Abuhassan, I. Petropavlovskikh, and G. McConville, (2015) Comparison of Ozone Retrievals from the Pandora Spectrometer System and Dobson Spectrophotometer in Boulder Colorado, Atmos. Meas. Tech., 8, 3407–3418, 2015 doi:10.5194/amt-8-3407-2015

Herman, Jay, Liang Huang, Richard McPeters, Jerry Ziemke, Alexander Cede, and Karin Blank, Synoptic ozone, cloud reflectivity, and erythemal irradiance from sunrise to sunset for the whole earth as viewed by the DSCOVR spacecraft from the earth–sun Lagrange 1 orbit, 2017, Atmos. Meas. Tech., 10, 1–18, https://doi.org/10.5194/amt-10-1-2017.

Ji, Q. and S.-C. Tsay (2000) On the dome effect of Eppley oyrgeometers and pyranometers, Geophys. Res. Lett.m 27:971-974.

Kopp, G.; Lean, J. L., (2011), A new, lower value of total solar irradiance: Evidence and climate significance, *Geophysical Research Letters*. **38**.

Littmann, Mark; Espenak, Fred; **Wilcox**, Ken (2008). Totality: Eclipses of the Sun. Oxford University Press. pp. 18–19. ISBN 0-19-953209-5.

Liendo, J.A. and G.H. Chacin, (2004), A study of a solar eclipse using a photocell, Revista Brasileira de Ensino de Fisica, v. 26, 395 – 399.

Maignan, F., Breon, F. M., and Lacaze, R., (2004), Bidirectional reflectance of Earth targets: Evaluation of analytical models using a large set of spaceborne measurements with emphasis on the Hot Spot, Remote Sens. Environ., 90, 210–220, doi:10.1016/j.rse.2003.12.006.

Marshak, Alexander, Jay R. Herman, Adam Szabo, Karin B. Blank, Alexander Cede, Simon A. Carn, Igor V. Geogdzhaev, Dong Huang, Liang-Kang Huang, Yuri Knyazikhin, Matthew G. Kowalewski, Nickolay A. Krotkov, Alexei I. Lyapustin, Richard D. McPeters, Omar O. Torres and Yuekui Yang, (2017), Earth Observations from DSCOVR/EPIC Instrument, BAMS, submitted.

Mayer, B. and Kylling, (2005) A.: Technical Note: The libRadtran software package for radiative transfer calculations: Description and examples of use, Atmos. Chem. Phys., 5, 1855–1877, http://www.atmos-chem-phys.net/5/1855/2005/.

Meeus, J. (2003). "The maximum possible duration of a total solar eclipse". *Journal of the British Astronomical Association*. **113** (6): 343–48.

Psiloglou, B.E. and H. D. Kambezidis, Performance of the meteorological radiation model during the solar eclipse of 29 March 2006, Atmos. Chem. Phys., 7, 6047–6059, 2007.

Wen, G., A. Marshak, and R.F. Cahalan, (2008) Importance of molecular Rayleigh scattering in the enhancement of clear sky radiance in the vicinity of boundary layer cumulus clouds. J. Geophys. Res., 113: [10.1029/2008JD010592].

Acknowledgement

The author would like to thank the DSCOVR project for support in completing this study as well as financial support from an accepted NASA-ROSES proposal in response to NNH16ZDA001N-ISE. All data is from the permanent NASA data repository:
https://eosweb.larc.nasa.gov/project/dscovr/dscovr_epic_l1b.